Theor Chem Acc (2012) 131:1244
DOI 10.1007/s00214-012-1244-5

REGULAR ARTICLE

Electron momentum spectroscopy of metal carbonyls: a reinvestigation of the role of nuclear dynamics

Balázs Hajgató · Filippo Morini · Michael S. Deleuze

Received: 14 February 2012 / Accepted: 5 June 2012 / Published online: 22 June 2012

Abstract The main purpose of this work is to reinvestigate the influence of nuclear dynamics in the electronic ground state of group 6 metal hexacarbonyl compounds [$W(CO)_6$, $Cr(CO)_6$, $Mo(CO)_6$] on electron momentum density profiles obtained from experimental orbital reconstructions employing Electron Momentum Spectroscopy. We call into question the view (Liu et al. in Chem Phys Lett 497:229, 2010) that thermally induced nuclear displacements associated with the first three triply degenerate $1T_{2g}$, $1T_{1u}$, and $1T_{2u}$ vibrational eigenmodes can be large enough at or near room temperature (298–310 K) to explain on their own the unexpectedly large electron densities inferred for the frontier orbitals of these compounds at low momenta. In this purpose, we resort to an analysis of populations over these three vibrational eigenmodes, according to a description of vibrational excitations employing Maxwell–Boltzmann statistical thermodynamics. Comparison is made with Born–Oppenheimer Molecular Dynamical (BOMD) simulations over the potential energy surface associated with the electronic ground state. The role of nuclear dynamics in the final ionized state, in the form of Jahn–Teller distortions, is also tentatively investigated.

Keywords Electronic structure theory · Electron Momentum Spectroscopy · Orbital imaging experiments · Electron impact (e, 2e) ionization · Distorted wave effects · Molecular dynamics · Statistical thermodynamics

Published as part of the special collection of articles celebrating theoretical and computational chemistry in Belgium.

B. Hajgató · F. Morini · M. S. Deleuze (✉)
Research Group of Theoretical Chemistry and Molecular Modeling, Hasselt University, Agoralaan Gebouw D, 3590 Diepenbeek, Belgium
e-mail: michael.deleuze@uhasselt.be

B. Hajgató
e-mail: hajgato@vub.ac.be

B. Hajgató
General Chemistry Division, QCMM Research Group, Alliance Ghent-Brussels, Free University of Brussels, Pleinlaan 2, 1050 Brussels, Belgium

Present Address:
B. Hajgató
Algemene Chemie, Vrije Universiteit Brussel, Pleinlaan 2, 1050 Brussels, Belgium

1 Introduction

Electron Momentum Spectroscopy [1–4] is a powerful orbital imaging technique, which enables straightforward reconstructions of electron momentum distributions associated with specific ionization channels (i.e., of orbital momentum profiles in a one-electron picture of ionization), according to an angular analysis of intensities in electron impact (e, 2e) ionization experiments [$M + e^- (E_0 + \varepsilon_b) \rightarrow M^+ + 2e^- (E_0/2)$] at high kinetic energies ($E_0 =$ 1.2 keV or more). The analysis of EMS experiments represents one of the main research topics of the theoretical chemistry research group at Hasselt University (Belgium) since 2000 (see e.g. Ref. [5]). Numerous approximations are required in this purpose. The first of these is the *Born–Oppenheimer (BO) approximation*, in which the coordinate-space representations of the initial and final states are products of separate electronic, vibrational and rotational functions. The corresponding (e, 2e) cross-sections are thereby obtained as transition amplitudes in between these states over the electron scattering potential [6, 7], which involves all electrons and nuclei in the molecular target. Upon invoking the *binary encounter approximation*, it is then

assumed that the momentum lost by the incident electron is entirely transferred to the ejected ones. Under these conditions, the transition operator depends solely upon the coordinates of the impinging electron and of the two ejected electrons. This approximation is designed for the kinematic situation on the Bethe ridge [1–4] where the momentum of the ionized electron is equal in magnitude to the momentum transferred from the incident to the scattered electron, ensuring thereby a clean "knock-out" process, a condition which is best satisfied experimentally by a symmetric non-coplanar set-up. In the framework of the *first Born* (or sudden) *approximation*, the incident electron is assumed to interact with the target *only once*. When the incident electron only interacts with the ejected electrons and neither affects the target nor is affected by the target, the *impulse approximation* is considered, and a simple relationships prevails between the azimuthal angle under which the electrons are collected and the momentum of the ejected electron *prior* to ionization. Modeling the incident and outgoing electrons as plane waves yields ultimately the *Plane Wave Impulse Approximation* (PWIA) [1–4], which implies that the energies of the unbound electrons are so high that their interactions with the residual ion are negligible. Upon the assumption that all these approximations are valid (e, 2e), ionization cross-sections for specific ionization channels in EMS conditions ultimately relate to spherically averaged and resolution folded structure factors that are obtained as the square of the Fourier Transform toward momentum space of the relevant *Dyson orbitals*, defined [8–11] as partial overlaps between the neutral initial ground state and final ionized state. A further and most useful approximation is the *target Kohn–Sham approximation* [12], which consists in substituting Dyson orbitals by the relevant Kohn–Sham orbitals, along with *ad hoc* or calculated spectroscopic pole strengths, in order to account for the flux of ionization intensity toward shake-up [13] and valence correlation bands [14] at higher electron binding energies. In many cases, (rescaled) Kohn–Sham orbitals are empirically known to be excellent approximations to Dyson orbitals [15, 16]. In practice, however, the interpretation of EMS experiments is subject to numerous complications such as: overlap effects in overcrowed ionization bands [17, 18], conformational mobility [19–21] and (thermally induced) nuclear dynamics in the electronic initial (neutral) ground state [22], shake-up processes due to electronic configuration interactions in the final ionized state [23–26], distorted wave and post-collision (e.g., rescattering) effects [27–33], and possibly ultra-fast nuclear dynamics in the final ionized state, in the form of bond breaking [22] or Coulomb explosion processes [34–36], as well as Jahn–Teller distortions [37] in the final ionized state.

Transition metal hexacarbonyls such as $W(CO)_6$, $Mo(CO)_6$, and $Cr(CO)_6$ are important precursors in organometallic chemistry [38–41]. Because of their high volatility and octahedral symmetry, they are also most useful molecular models for studies of bond formation between carbonyl groups and metal surfaces. Investigations of the outermost valence orbitals of these compounds comprise the ultra-violet [He I, He II] and X-ray photoelectron experiments by Higginson et al. [42] and various studies [43–45] employing Electron Momentum Spectroscopy (EMS). In the EMS studies of $Cr(CO)_6$, $Mo(CO)_6$, and $W(CO)_6$ by Chornay et al. [43], and by Rolke et al. [44], the measured (e, 2e) ionization cross-sections for the HOMO were found to be much larger than expected in the low momentum region, according to standard theoretical models of (e, 2e) ionization processes in the high energy limit, and to be largely inconsistent with the nodal characteristics of an uncorrelated (Hartree–Fock) $2t_{2g}$ orbital at $p = 0$. Within the framework of the Plane Wave Impulse Approximation [1–3], and from symmetry considerations, the spherically averaged momentum density of the HOMO of these three compounds is indeed expected to identically vanish at zero electron momentum, outside of a marginal contribution arising from finite angular resolution effects, that is, from experimental limitations in momentum resolution. On the contrary, particularly large "turn-ups" of the frontier electron densities were experimentally observed in the low momentum region [43, 44]. Accounting for electronic correlation in the ground state by means of the target Kohn–Sham approximation did not improve significantly the agreement between theory and experiment. This was expected, since the same symmetry constraints apply in Hartree–Fock and Density Functional Theories. By analogy with EMS experiments on atomic targets and calculations employing the Distorted Wave Impulse Approximation (DWIA [1–3]) of the Xe 4d, Cr 3d, Ti 3d and Mo 4d (e, 2e) ionization cross-sections [46], it was tentatively concluded [43, 44] that these discrepancies between theory and experiment are due to a breakdown of the plane wave impulse approximation and distorted wave effects in the continuum, which are known indeed nowadays [47] to be particularly significant when the ionized molecular orbital has a d-type topology (i.e., two perpendicular nodal planes).

However, the more recent EMS experiments by K. Liu et al. [45] on $W(CO)_6$ at electron impact energies of 1.2 and 2.4 keV gave at first glance quite similar momentum profiles for the HOMO and led thus on the contrary to the conclusion that distorted wave and post-collision effects are too weak to explain the experimentally observed turn-ups at low electron momenta. Since the target compounds contain relatively heavy metal atoms, this discrepancy between theory and experiment was then also thought to be the outcome of the limitations inherent to a non-relativistic depiction. Further investigations of scalar relativistic and spin–orbit coupling effects indicated, however, a very

marginal influence of these effects upon the computed momentum distributions [45]. In their ultimate attempt to reconcile theory with experiment, Liu et al. [45] invoked large-amplitude structural distortions in the form of wagging or bending motions associated with the three lowest and triply degenerate vibrational frequencies and the corresponding $1T_{2u}$, $1T_{1u}$, and $1T_{2g}$ eigenmodes (Fig. 1), regardless of anharmonic effects and of excessive energy demands resulting from exacerbated electrostatic repulsions between strongly polarized C=O substituents. In their study, it was simply assumed that thermally induced nuclear dynamics in the electronic ground state can be conveniently described by displacing nuclei away from their equilibrium position, according to so-called normalized vibrational eigenvectors (i.e., to eigenvectors the norm of which amounts to 1 $Å^2$, according to the ADF output for atomic displacements), and averaging thereby the obtained momentum distributions for the first three $1T_{2u}$, $1T_{1u}$, and $1T_{2g}$ eigenmodes. The main argument by Liu et al. [45] in support to their approach was that the population of the vibrational ground state accounts for less than 10 % of the total vibrational populations of the three lowest eigenmodes, at an estimated experimental temperature of 310 K, according to (Maxwell-) Boltzmann statistics. With this simple depiction of nuclear dynamics in the electronic ground state, Liu et al. [45] managed to obtain a much better match between theory and experiment and claimed therefore the case of the frontier orbital momentum distributions of $W(CO)_6$ to be understandable in terms of low-frequency vibrations. However, the extreme crudeness of their approach makes us believe that it is certainly worth reconsidering in details whether their analysis can resist more thorough analyses of thermally induced vibrational motions in the electronic ground state, and re-evaluate whether the observed discrepancies between the theoretical and experimental orbital momentum densities of group 6 metal hexacarbonyls are not at the end of the day the outcome of still unaccounted physical complications, such as ultra-fast nuclear dynamics in the final ionized state, or distorted wave and post-collision effects in the continuum.

At this stage, we wish to emphasize that so far an exact treatment of distorted wave effects for polyatomic systems remains intractable as it requires a multi-centre expansion of the continuum states in terms of Coulomb waves [48, 49]. Rigorous enough theoretical studies of distorted wave effects are nowadays only tractable for atomic targets [50], diatomic molecules (e.g., H_2 [30]), and small molecules such as H_2O [51]), the electron densities of which approach spherical symmetry, which enables slowly converging but highly accurate expansions of their molecular orbitals in a basis of *s*, *p*, *d*, *f*, *g* … atomic orbitals with varying exponents but with all the same location on the central "heavy" (O) atom. Note that highly qualitative theoretical studies of triple differential cross-sections for electron impact ionization experiments upon larger polyatomic systems (formic acid, methane, tetrahydrofurane, pyrimidine, …) using a three-body distorted wave model have also been reported recently (see [52] and references therein). A most serious drawback of these latter studies is that orientational averages of molecular orbitals (OAMOs) are used to represent the target bound state wave function, which means that the information associated with the nodal structure of the orbitals is almost entirely lost in the modeling of the distorted wave effects. In particular, OAMOs identically vanish at every point in space, except if the target bound state has the full symmetry of the molecular symmetry point group. Clearly, distorted wave effects from large polyatomic systems are still awaiting a satisfactory enough theoretical treatment.

The first purpose of the present work is thus to evaluate whether the structural distortions which were proposed by Liu et al. [45] are compatible with thermal fluctuations at or near standard room temperature, that is, at 298 and 310 K, according to Maxwell–Boltzmann (MB) statistics [53, 54] on vibrational energy levels. The analysis is supplemented by Born–Oppenheimer Molecular Dynamical (BOMD) simulations [55–57] at the same temperatures of momentum profiles inferred from *vertical* (e, 2e) ionization cross-sections. A main advantage of this approach is that, by virtue of ergodicity [58], it enables a complete exploration of phase space which is equivalent to an ensemble

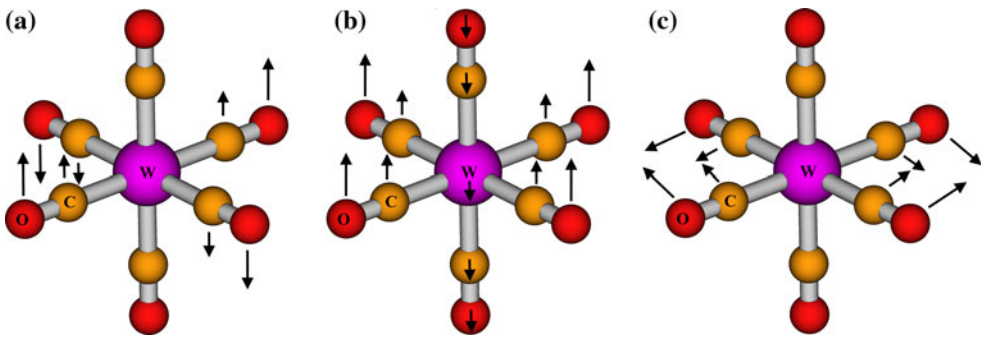

Fig. 1 The three lowest vibrational eigenmodes of $W(CO)_6$ (B3LYP/aug-cc-pVTZ-PP level): **a** 59.5 cm^{-1}, **b** 81.7 cm^{-1}, and **c** 84.3 cm^{-1}

average over all internal degrees of freedom of the system of interest, such as is computed in Monte Carlo simulations. Born–Oppenheimer Molecular Dynamics is therefore the most convenient approach for a realistic description of the intrinsically chaotic nature of nuclear motions in a large polyatomic system, taking into account non-harmonic effects (anharmonicities in the vibrational potentials, couplings between vibrations and rotations, couplings between internal and external rotations due to Coriolis forces, …) in the classical approximation. The interested reader is referred in particular to studies of non-harmonic effects in infra-red vibrational spectra, obtained by Fourier transforming to the energy domain dipole time-dependent autocorrelation functions inferred from BOMD simulations [59–62].

To our knowledge [63], there is no way to precisely control the temperature with the current experimental (e, 2e) setup which Liu et al. [45] used at Tsinghua University (Beijing, China) for their experiments on $W(CO)_6$, a set-up which employs effusive molecular beams. In contrast with experiments based on free expansions in supersonic jets, it is usually assumed that the relatively high pressure in the collision cell ensures a full randomization of molecular motions, and thermal equilibrium therefore with the environment (298 K). Therefore, we wish to consider both the estimated experimental and standard room temperatures in our BOMD analysis. At last, the role played by nuclear dynamics in the final ionized state is also tentatively investigated. In this purpose, we revise before all (theory section) how electron momentum distributions may vary in response to a change in the molecular geometry induced by ionization.

2 Theory

Within the framework of the Born–Oppenheimer, binary encounter, plane wave impulse and target Kohn–Sham [KS] (or target Hartree–Fock [HF]) approximations, and disregarding rotational wave functions, differential (e, 2e) ionization cross-sections are proportional to the square of a structure factor $F_n(\vec{p})$, which is given by [1–3, 64]:

$$F_n(\vec{p}) = \int dQ\; X^*_{\upsilon'}(Q)\; X_{\upsilon}(Q)\; S_n(Q)\; \varphi_i(\vec{p}, Q). \tag{1}$$

In the above equation, Q is the set of internal coordinates determining the displacements from equilibrium of atomic nuclei in the molecule, $X_{\upsilon}(Q)$ and $X_{\upsilon'}(Q)$ are the vibrational wave functions corresponding to the initial (neutral) ground state $[\Psi_0^N(Q)]$ and final ionized state $[\Psi_n^{N-1}(Q)]$ of the molecule, $\varphi_i(\vec{p}, Q)$ is the Fourier transform to momentum space of the target KS or HF orbital $[\varphi_i(\vec{r}, Q)]$ in the initial (neutral) ground state, and $S_n(Q)$ is the overlap integral of the electronic wave functions for the final ionized state and the electronic residue left after annihilating an electron from the target orbital $\varphi_i(\vec{r}, Q)$:

$$S_n(Q) = \left\langle \Psi_n^{N-1} \middle| a_i \middle| \Psi_0^N \right\rangle, \tag{2}$$

with a_i the relevant annihilation operator, and where N represents the number of electrons in the target molecule. Upon carrying integrations over vibrational coordinates, Eq. (1) can be further reduced to [1, 3, 64]:

$$F_n(\vec{p}) = g_{\upsilon}^{\upsilon'}\; S_n(\bar{Q})\; \varphi_i(\vec{p}, \bar{Q}), \tag{3}$$

where $g_{\upsilon}^{\upsilon'} = \int dQ\; X^*_{\upsilon'}(Q)\; X_{\upsilon}(Q)$ is the usual Franck–Condon factor, and $\bar{Q}$ represent *some mean values of nuclear coordinates that are intermediate* between the equilibrium coordinates of nuclei Q_0 and Q'_0 in the initial neutral ground state and final ionized state, respectively. Vibrational states are most commonly unresolved in Electron Momentum Spectroscopy, which enables us to derive the relevant (e, 2e) ionization cross-sections from the spherical average:

$$\sigma^{\mathrm{EMS}} \propto \left|S_n(\bar{Q})\right|^2 \int \mathrm{d}\Omega_{\vec{p}}\; \left|\varphi_i(\vec{p}, \bar{Q})\right|^2, \tag{4}$$

with $d\Omega_{\vec{p}}$ an infinitesimal element of solid angle associated with the target electron momentum, and where $\left|S_n(\bar{Q})\right|^2$ represents the spectroscopic strength of the electronic transition $[\Psi_0^N(\bar{Q}) + 1e^- \rightarrow \Psi_n^{N-1}(\bar{Q}) + 2e^-]$ of interest.

At high enough impact electron energies, it is most customary to assume a *vertical* ionization process, in which case $\bar{Q} = Q_0$. Due to the long-range character of the Coulomb force and wave packet nature of the impinging electron, deviations from a vertical transition can*not* be systematically ruled out in (e, 2e) ionization experiments. At another extreme, when nuclear dynamics is expected to compete with (i.e., to be faster than) the (e, 2e) ionization process, one may thus empirically resort to an *adiabatic* depiction, in which case $\bar{Q} = Q'_0$. Such rare situations may typically occur with Jahn–Teller distortions associated with conical intersections, which are known to generally yield a non-radiative decay of the upper electronic state within the femtosecond regime [65, 66], that is, within a time scale which is comparable to the effective time scale inferred recently in studies of bond dissociation processes [67] induced by (e, 2e) ionization processes at electron impact energies around 1.2 keV.

3 Methodology

The geometry optimizations as well as the vibrational and dynamical analyses which are reported in the sequel have been performed using Density Functional Theory (DFT)

[68] in conjunction with the standard hybrid Becke-3-parameters-Lee–Yang–Parr [B3LYP] functional [69, 70], or the dispersion-corrected ωB97XD exchange–correlation functional [71]. Our main motivation for using a dispersion-corrected functional is to enable a proper treatment of non-bonded interactions between carbonyls. In all our calculations upon group 6 [W, Mo, Cr] hexacarbonyls, use was made of the aug-cc-pVDZ and aug-cc-pVTZ basis sets [72, 73] for the carbon and oxygen atoms. Chromium was also described using the all-electron aug-cc-pVDZ and aug-cc-pVTZ basis sets. Relativistic effects arising from the chemically inert cores of Mo and W were accounted for through the interplay of accurately designed pseudo-potentials (PPs). Specifically, the Mo atom was described by the ECP28MDF energy-consistent effective pseudopotential, which was constructed from a multi-state fit of a fully relativistic Dirac–Fock calculation for the isolated atom [74], together with the correspondingly adjusted correlation consistent aug-cc-pVDZ-PP and aug-cc-pVTZ-PP basis sets. The energy-consistent effective core potential ECP60MDF [75] has been adopted for the tungsten atom in conjunction with its accompanying correlation consistent aug-cc-pVDZ-PP and aug-cc-pVTZ-PP basis sets. Although this goes much beyond our present purpose, it is worth noting that errors arising from the use of these pseudo-potentials are effectively extremely small and comparable to the accuracies that can be achieved nowadays with modern all-electron ab initio calculations. Comparison to large basis set, all electron, relativistic calculations indicate errors of $\sim$0.002 Å only in equilibrium bond lengths and less than 0.5 kcal/mol in dissociation energies, due to the pseudo-potential approximation [76]. Along with standard gradient-corrected hybrid functionals (e.g., B3LYP), effective relativistic small-core pseudo-potentials are known also to enable insight into vibrational frequencies within a few cm^{-1} accuracy [77]. For our purpose, the main advantage of these pseudo-potentials is mainly to enable the computation of analytic energy gradients and, thus, of molecular dynamical trajectories on accurate enough potential energy surfaces, which are still to date beyond reach in a fully relativistic treatment. All DFT calculations presented in this work were performed by means of the Gaussian09 package of programs [78].

In this work, we simulate the outcome of EMS experiments upon $W(CO)_6$ using a standard (e, 2e) non-coplanar symmetric kinematical setup at an electron impact energy of 2.4 keV above the vertical ionization energy threshold (VIE $\sim$ 8.6 eV). According to the characteristics of the (e, 2e) spectrometer [79] which was employed by Liu et al. at Tsinghua University (Beijing) [45], the relevant parameters for the momenta of the impinging and outgoing electrons amount therefore to $p_0 = 0.271105(2400 + \mathrm{VIE})^{1/2}$ au (1 au = 1 a_0^{-1}, with a_0 as the Bohr radius, that is, 0.5292 Å) and $p_1 = p_2 = 9.39135$ au, respectively ($E_1 = E_2 =$ 1,200 eV). The binary (e, 2e) encounter, plane wave impulse, and target Kohn–Sham approximations are invoked in conjunction with calculations employing DFT and the B3LYP or ωB97XD functionals. Deviations from basis set completeness (BSC) are checked by comparing results employing the aug-cc-pVDZ-PP and aug-cc-pVTZ-PP basis sets. It is worth reminding that Kohn–Sham orbitals and their energies are known to represent valuable approximations to the corresponding Dyson orbitals and (electronically relaxed) ionization energies produced in CI (Configuration Interaction) calculations [80, 81], and that, by virtue of Janak's theorem [82] or the extended Koopmans' theorem [83], the approximation becomes exact when considering specifically the HOMO and an (hypothetical) exact exchange–correlation functional.

Spherically averaged orbital momentum distributions have been generated from the obtained Kohn–Sham orbitals using the MOMAP program by Brion and coworkers [84] and homemade interfaces. In line with the study by Liu et al. [45], and employed (e, 2e) spectrometer therein, resolution folding of the computed momentum distributions was made using a Monte Carlo simulation procedure [85, 86], considering angular resolutions of 0.53° and 0.84° on azimuthal and polar angles, respectively. For the sake of consistency with the EMS experiments by Rolke et al. [44], the following parameters have been retained for the simulation of the outermost (e, 2e) momentum profiles of $Mo(CO)_6$ and $Cr(CO)_6$: $E_0 = 1{,}200$ eV, $\Delta\theta = 0.60°$, and $\Delta\phi = 1.20°$.

In all BOMD simulations, the Bulirsch-Stoer method was used for the integration scheme [87, 88], along with an integration step size of 0.2 fs, and using a fifth-order polynomial fit in the integration correction scheme. The trajectory step size was set to 0.250 a.u, and atomic coordinates were dumped at time intervals of approximately 1 fs. Thermalization to standard room temperature (298 K) was ensured by setting the initial rotational energy from a thermal distribution assuming a symmetric top. The time average was made on momentum densities computed at each point of the calculated BOMD trajectory in the MD run. Runtimes comprised between 1.5 and 1.7 ps, corresponding to time averages over 1,500–1,700 thermally distorted structures.

In line with equation 4, the influence of nuclear dynamics in the final ionized state has been tentatively and phenomenologically investigated upon the assumption of an adiabatic ionization process, by computing (resolution folded and spherically averaged) frontier electron momentum profiles for the target orbitals in the initial neutral ground state upon nuclei configurations corresponding to all possible equilibrium geometries of the final

cationic state ($\bar{Q} = Q_0^{'}$). The approach we consider in this purpose is therefore the same as that used recently by Chen XJ and his co-workers [37] for unraveling the outcome of Jahn–Teller distortions in EMS experiments upon cyclopropane, which were found to leave clearly identifiable fingerprints in the frontier (e, 2e) ionization bands and the correspondingly inferred electron momentum distributions. It is worth noting that, by virtue of the equations presented in section II, such an approach will clearly provide *upper estimates* to the changes in momentum profiles due to vibronic coupling interactions induced by the (e, 2e) ionization processes. Molecular structures and orbital contours were drawn using the MOLDEN program [89].

4 Results and discussion

Prior to any further discussion, it is worth considering the integrated (e, 2e) ionization spectrum of $W(CO)_6$ recorded by Liu et al. [45] (Fig. 2). Upon examining this spectrum, it is clear that the momentum distribution characterizing the HOMO ($2t_{2g}$) is free of any unwanted complications related to band overlaps [18] and that individual Jahn–Teller components remain unresolved. Also (Fig. 3), this momentum distribution is almost insensitive to the employed functional. Compared with the aug-cc-pVDZ(-PP) basis set, the aug-cc-pVTZ(-PP) basis set appears to be large enough to ensure the required saturation of results toward the BSC limit. Our momentum profiles are also almost identical to results obtained by Liu et al. [45], according to B3LYP relativistic calculations coping with scalar relativistic and spin–orbit coupling interactions at the level of the zero-order regular approximation (ZORA [90]) using a specifically designed triple-zeta doubly polarized basis set.

All B3LYP calculations (including frequency calculations) by Liu et al. [45] were performed upon the MP2 geometry which was optimized by Ehlers and Frenking [91], using an effective core potential [92] and the (441/2111/2) valence basis set derived from the minimal Hay–Wadt (55/5/3) basis set [93] on the tungsten atom and the 6-31G* basis set [94] on carbon and oxygen atoms. This methodological inconsistency resulted into a rather significant underestimation of the W–C and C–O bond lengths by 0.0125 Å and 0.025 Å, respectively, compared with the methodologically correct B3LYP values. Since the B3LYP vibrational calculations by Liu et al. [45] were performed away from the global energy minimum, they resulted (Table 1) in much too large values (by $\sim$40 % or more) for the frequencies characterizing the three lowest and triply degenerate vibrational eigenmodes ($1T_{2u}$, $1T_{1u}$, $1T_{2g}$), compared with experiment—an overestimation which has in turn most clearly led to further severe errors in

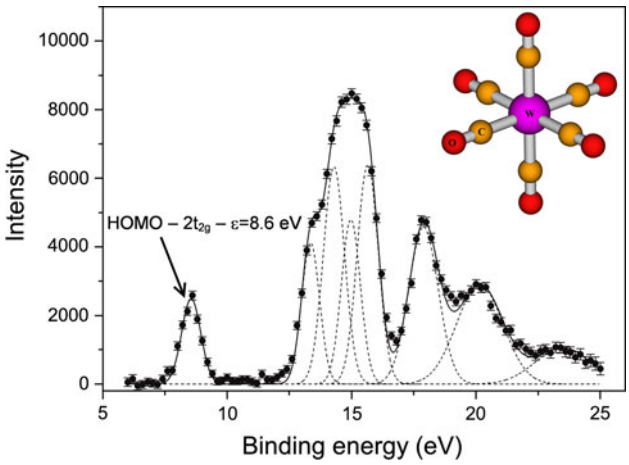

Fig. 2 Experimental electron momentum spectrum [45] of $W(CO)_6$ summed over all angles ($E_0 = 1{,}200$ eV, $\Delta\theta = 0.53°$, $\Delta\phi = 0.84°$)

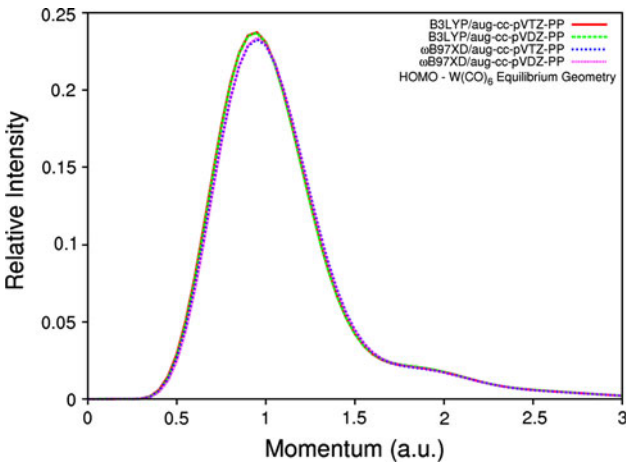

Fig. 3 Spherically averaged theoretical momentum profiles (without resolution folding) of the HOMO of $W(CO)_6$

the computations of vibrational populations. A further consequence of using a non-stationary point on the potential energy surface is that nuclear displacements characterizing normalized vibrational eigenmodes have also been certainly overestimated. In contrast, our theoretical estimates for vibrational frequencies, in particular, the B3LYP ones, are in remarkable agreement with the available experimental values [95, 96], as well as with the results of quasi-relativistic (QR) DFT calculations [97] employing GGA functionals. Deviations between our results, the QR-GGA results by Bérces and experiment for the three modes of interest does not exceed 6 cm^{-1}.

Although vibrations of the order of 60–80 cm^{-1} are not uncommon at all in organic and inorganic compounds, Liu et al. [45] considered these to be indicative of a very shallow energy minimum on the potential energy surface,

Table 1 Lowest vibrational frequencies (in cm^{-1}) of $W(CO)_6$

Mode	Liu et al.[a]	B3LYP/aug-cc-pVTZ-PP	ωB97XD/aug-cc-pVTZ-PP	GGA + QR[b]	Experimental[c]
t_{2u}	100.3	59.5	55.8	63.6	61 ± 15[d]
t_{1u}	133.5	81.7	79.3	80.8	82.0 ± 3[e]
t_{2g}	120.8	84.3	81.6	85.9	88.3 ± 6[f]

[a] From Ref. [45]

[b] From Ref. [97]

[c] From Refs. [95] and [96]

[d] Raman, solid phase, from overtone combination

[e] IR, gas phase

[f] Raman, liquid phase

that would therefore permit extremely large atomic displacements, away from the minimum, due to thermal fluctuations and vibrational excitations in the electronic ground state, and would provide a convenient way to describe nuclear dynamics in the electronic neutral ground state. In support to these assertions, Liu et al. calculated relative populations for the ground ($n = 0$) and vibrationally ($n > 0$) excited states, on the ground of (Maxwell-)Boltzmann statistics [98–100]:

$$p_n(i) = \frac{g_n(i)}{\exp(\varepsilon_n/kT)} = \frac{g_n(i)}{\exp([n+1/2]hv_i/kT)}, \quad (5)$$

with n the relevant vibrational quantum number ($n = 0$, 1, 2, 3 …), and $g_n(i)$ the multiplicity factor proposed by Herzberg [101] for triply degenerate vibrations:

$$g_n(i) = \frac{1}{2}(n+1)(n+2). \quad (6)$$

Since the vibrational eigenmodes (i) of interest exhibit frequencies in the 60–100 cm^{-1} range, and characteristic temperatures ($\theta_i = hv_i/k$) of the order of 86 to 144 K only, the Boltzmann approximation can be regarded as valid at and above room temperature ($T = 298$ K). With this approximation, inversions of relative populations are observed at around $n = 6$, 4 and 3 for the $1T_{2u}$, $1T_{1u}$, and $1T_{2g}$ vibrational modes (Table 2), respectively.

The analysis by Liu et al. [45] simply accounts for thermal distortions of the molecular structure in the electronic ground state by arbitrarily displacing atoms according to so-called *normalized* vibrational displacements for the first three eigenmodes, and averaging the ultimately obtained momentum distributions. We remind that these normalized displacements are nothing else than vibrational eigenmodes taken from the ADF output, the norms of which are equal to 1 $Å^2$. This approach obviously neglects anharmonic effects and the excessive energy penalties resulting from the imposed structural distortions, because of electrostatic repulsions between strongly polarized CO substituents, due to bond donation to the group 6 metal (the same considerations on charge transfers also prevail for $Mo(CO)_6$ and $Cr(CO)_6$—see natural atomic charges in Table 3). To quantitatively investigate these penalties, we refer the reader to Table 4, in which each listed configuration ($\alpha = 0.0, 0.1, 0.2, 0.3 \ldots 1.0$) is the one obtained by adding to the nuclear coordinates characterizing the O_h energy minimum form nuclear displacements taken to be equal to α times the relevant and so-called "normalized" eigenmode (see above definition, following the conventions used by Liu et al. [45]). Calculations at the B3LYP/aug-cc-pVTZ-PP level (Table 5) of the corresponding anharmonic energy demands and required thermal fluctuations are conclusive enough for refuting the view that normalized vibrational eigenmodes enable a consistent description of thermally induced vibrational motions in the electronic ground state. Indeed, upon considering the obtained energy values, it is clear that thermal fluctuations at or near room temperature are consistent with α factors ranging from ~0.3 to ~0.5, whereas in normal conditions, a full "normalized" displacement ($\alpha = 1$) is thermodynamically unreachable (since the corresponding energy demands would imply thermal fluctuations ranging

Table 2 Relative population occupations [$p_n(i)$] of the three lowest vibrational levels of $W(CO)_6$ at 298.15 K arising from the first three eigenmodes (harmonic approximation, Boltzmann statistics, B3LYP/aug-cc-pVTZ(-PP) results)

Vib. level (n)	t_{2u}	t_{1u}	t_{2g}
0	1.0000	1.0000	1.0000
1	2.2511	2.0222	1.9973
2	3.3783	2.7262	2.6594
3	4.2250	3.0627	2.9508
4	4.7554	3.0966	2.9467
5	4.9957	2.9223	2.7465
6	4.9981	2.6264	2.4380
7	4.8220	2.2762	2.0868
8	4.5228	1.9178	1.7366
9	4.1480	1.5800	1.4131

Table 3 Natural atomic charges

$W(CO)_6^a$		$Mo(CO)_6^b$		$Cr(CO)_6^c$	
Atom	Charge	Atom	Charge	Atom	Charge
W	−2.26677	Mo	−2.12850	Cr	−2.55633
C	0.80226	C	0.79384	C	0.87483
C	0.80226	C	0.79384	C	0.87483
C	0.80226	C	0.79384	C	0.87483
C	0.80226	C	0.79384	C	0.87483
C	0.80226	C	0.79384	C	0.87483
C	0.80226	C	0.79384	C	0.87483
O	−0.42446	O	−0.43909	O	−0.44877
O	−0.42446	O	−0.43909	O	−0.44877
O	−0.42446	O	−0.43909	O	−0.44877
O	−0.42446	O	−0.43909	O	−0.44877
O	−0.42446	O	−0.43909	O	−0.44877
O	−0.42446	O	−0.43909	O	−0.44877

[a] B3LYP/aug-cc-pVTZ(-PP)

[b] B3LYP/aug-cc-pVDZ(-PP)

[c] B3LYP/aug-cc-pVDZ

from 2,500 to 8,000 K). For the $1T_{2u}$ mode, a temperature of about 450 K is required (Table 5) for increasing the population of the relevant vibrational levels ($n = 31, 32$) relative to the vibrational ground state above a significant enough threshold (100 %). At this temperature, the relative population of the relevant vibrational levels ($n = 70, 71$) or ($n = 37, 38$) for the $1T_{1u}$ and $1T_{2g}$ modes are still below 0.005 and 0.5 %, respectively (Table 5). Clearly, at or near room temperature, it makes no sense to simply consider nuclear displacements amounting to a "normalized" vibrational eigenmode for unraveling the outcome in EMS expertiments of low-frequency vibrational motions in tungsten hexacarbonyl, especially for the $1T_{1u}$ and $1T_{2g}$ modes, because of the high energy demand required by excitations to vibrational quanta that correspond to exceedingly large displacements.

Different theoretical models of nuclear dynamics in the initial state are tested in Figs. 4 and 5 and compared (Fig. 5) against the experimental electron momentum distributions inferred by Liu et al. [45] for the HOMO ($2t_{2g}$ orbital) of tungsten hexacarbonyl. In line with the latter work, molecular vibrations in the ground state are first accounted for by averaging the outcome of normalized ($\alpha = 1$) and rescaled ($\alpha = 0.4$) nuclear displacements. As was noted by Liu et al. [45], whereas vanishing (e, 2e) ionization intensities are expected for the HOMO at $p \rightarrow 0$ for the ground state octahedral energy minimum form of tungsten hexacarbonyls, enforcing normalized nuclear displacements results into a significant enhancement [i.e., a turn-up (using the technical jargon in use for 2–3 decades already in the EMS community)] of frontier momentum densities in the low momentum region. Note nonetheless that in our case, the predicted increase of (e, 2e) ionization intensities at $p \rightarrow 0$ when $\alpha = 1$ is still far from enabling us to fully reproduce the experimentally obtained momentum densities in the low momentum region. Results obtained upon properly rescaled ($\alpha = 0.4$) nuclear displacements for the first three eigenmodes ($1T_{2u}$, $1T_{1u}$, $1T_{2g}$) demonstrate that, at room temperature, these molecular vibrations in the electronic ground state can on their own certainly not be at the origin of the experimentally observed turn-up in momentum densities at low momenta. As a matter of fact, there is almost no discernable difference in between these latter results and the momentum profile calculated for the HOMO upon using the equilibrium geometry of $W(CO)_6$.

Table 4 Anharmonic energy demands and thermal fluctuations associated with distortions associated with the first three normal vibrational modes of $W(CO)_6$ (B3LYP/aug-cc-pVTZ-PP results, see text for a definition of the scaling factor α)

α	t_{2u}			t_{1u}			t_{2g}		
	Energy (kcal/mol)	Energy (cm^{-1})	Energy (K)	Energy (kcal/mol)	Energy (cm^{-1})	Energy (K)	Energy (kcal/mol)	Energy (cm^{-1})	Energy (K)
0.0	0.00	0.0	0	0.00	0.0	0	0.00	0.0	0
0.1	0.06	21.0	30	0.06	19.3	28	0.05	16.7	24
0.2	0.13	45.6	66	0.24	82.5	119	0.20	68.7	99
0.3	0.26	91.2	131	0.59	205.4	296	0.46	161.9	233
0.4	0.47	164.6	237	1.18	413.6	595	0.87	305.8	440
0.5	0.79	275.2	396	2.12	741.5	1,067	1.47	513.7	739
0.6	1.24	434.7	625	3.52	1,230.8	1,771	2.29	802.0	1,154
0.7	1.88	657.0	945	5.51	1,928.2	2,774	3.40	1,189.8	1,712
0.8	2.74	957.9	1,378	8.25	2,884.0	4,150	4.86	1,698.6	2,444
0.9	3.87	1,354.3	1,949	11.86	4,149.6	5,971	6.72	2,351.7	3,384
1.0	5.33	1,864.6	2,683	16.51	5,775.9	8,311	9.07	3,173.3	4,566

Table 5 Fractional populations of vibrational levels (n) approaching a normalized vibrational displacement (i.e., $\alpha = 1$), relative to the ground state ($n = 0$)

T (K)	n	t_{2u} E_v (cm^{-1})	Relative fraction	n	t_{1u} E_v (cm^{-1})	Relative fraction	n	t_{2g} E_v (cm^{-1})	Relative fraction
298	31	1,845	7.18×10^{-2}	70	5,721	2.61×10^{-9}	37	3,119	2.15×10^{-4}
	32	1,904	5.72×10^{-2}	71	5,803	1.81×10^{-9}	38	3,204	1.51×10^{-4}
310	31	1,845	1.01×10^{-1}	70	5,721	7.51×10^{-9}	37	3,119	3.82×10^{-4}
	32	1,904	8.14×10^{-2}	71	5,803	5.28×10^{-9}	38	3,204	2.72×10^{-4}
320	31	1,845	1.32×10^{-1}	70	5,721	1.72×10^{-8}	37	3,119	6.01×10^{-4}
	32	1,904	1.07×10^{-1}	71	5,803	1.23×10^{-8}	38	3,204	4.33×10^{-4}
330	31	1,845	1.70×10^{-1}	70	5,721	3.75×10^{-8}	37	3,119	9.20×10^{-4}
	32	1,904	1.39×10^{-1}	71	5,803	2.70×10^{-8}	38	3,204	6.70×10^{-4}
350	31	1,845	2.69×10^{-1}	70	5,721	1.56×10^{-7}	37	3,119	2.00×10^{-3}
	32	1,904	2.23×10^{-1}	71	5,803	1.15×10^{-7}	38	3,204	1.49×10^{-3}
400	31	1,845	6.93×10^{-1}	70	5,721	2.95×10^{-6}	37	3,119	9.94×10^{-3}
	32	1,904	5.95×10^{-1}	71	5,803	2.26×10^{-6}	38	3,204	7.72×10^{-3}
450	31	1,845	1.45×10^{0}	70	5,721	2.91×10^{-5}	37	3,119	3.46×10^{-2}
	32	1,904	1.27×10^{0}	71	5,803	2.30×10^{-5}	38	3,204	2.78×10^{-2}

Born–Oppenheimer Molecular Dynamical simulations of atomic trajectories over the ωB97XD/aug-cc-pVTZ potential energy surface associated with the electronic ground state of $W(CO)_6$ and a time average over the 1,500–1,600 thermally distorted structures dumped from these simulations enables us to account on classical grounds for the contribution of all 33 vibrational eigenmodes of this compound in an anharmonic depiction as well as of their coupling with internal and external rotations, due for instance to Coriolis forces. Increasing the temperature from 298 and 310 K does not make in practice any observable difference in the ultimately obtained spherically averaged and resolution folded momentum distributions. When accounting with molecular dynamics for all vibrational and rotational degrees of freedom, a significantly stronger turn-up at low momentum is observed in the momentum distribution characterizing the HOMO (Fig. 5). This turn-up is, however, far to be strong enough to quantitatively reproduce the experimental profile in this region. Upon scrutinizing in details the results of our BOMD simulations at or near room temperature, it appears that the thermally induced structural distortions which have the most pronounced effect at low momenta correspond to bending of the W–C–O bond angles.

Similar remarks can be made regarding the influence of nuclear dynamics in the initial ground state upon the momentum profile characterizing the HOMO of $Cr(CO)_6$ and $Mo(CO)_6$. As our results indicate (Figs. 6, 7), compared with the available measurements, nuclear dynamics in the initial state is found in both cases to yield a

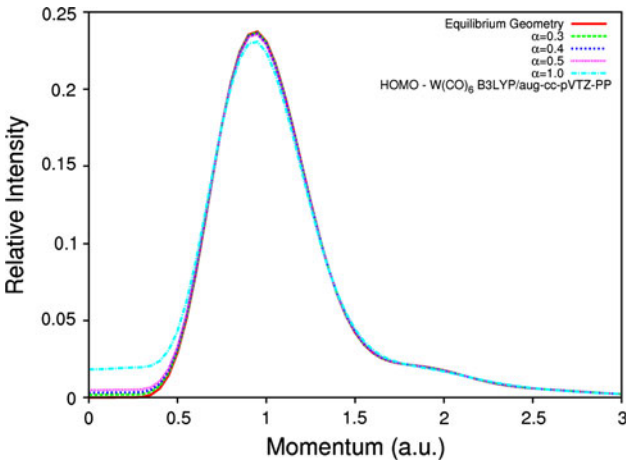

Fig. 4 Study of the consequences of structural distortions along the three first vibrational eigenmodes of $W(CO)_6$ upon the momentum profile characterizing the HOMO (without resolution folding). See text and Table 4 for a definition of the scaling factor α (results of single point calculation results at the B3LYP/aug-cc-pVTZ-PP level)

significant albeit too weak turn-up of the frontier momentum densities at low momenta.

Starting from the vertical ionized state, the adiabatically relaxed molecular structures of the radical cation of the $M(CO)_6$ compounds (M=Cr, Mo, W) were found by systematically imposing tiny atomic displacements in the directions indicated by the vibrational eigenmodes associated with imaginary frequencies, and releasing thereafter all symmetry constraints during the geometry optimization process. Visual inspection along with careful verifications employing frequency analysis indicate that the molecular

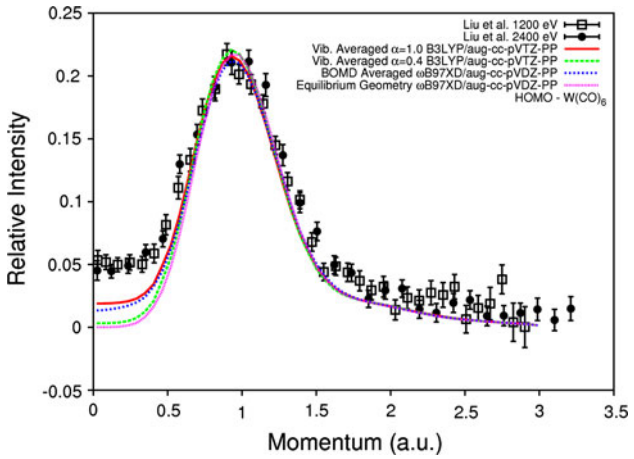

Fig. 5 Resolution folded ($E_0 = 2{,}400$ eV, $\Delta\theta = 0.53°$, $\Delta\phi = 0.84°$) and spherically averaged theoretical momentum distribution inferred for the HOMO of $W(CO)_6$ ($\varepsilon = 8.6$ eV), taking care of complications pertaining to nuclear dynamics in the initial state

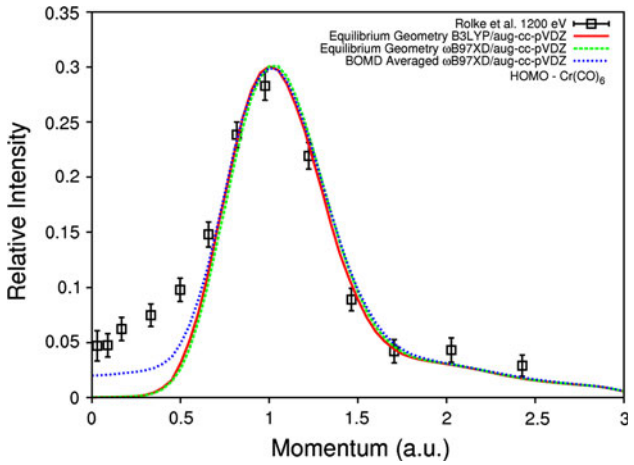

Fig. 6 Resolution folded ($E_0 = 1{,}200$ eV, $\Delta\theta = 0.60°$, $\Delta\phi = 1.20°$) and spherically averaged theoretical momentum distribution inferred for the HOMO of $Cr(CO)_6$ ($\varepsilon = 8.4$ eV), taking care of complications pertaining to nuclear dynamics in the initial state

structure of the radical cation of group 6 metal hexacarbonyl compounds can be discussed in terms of two structures of D_{3d} symmetry, which essentially differ by the extent of the angle (τ) in between the C–M bonds and the remaining C_3 rotation axis (Fig. 8). In these structures, the central metal, carbon and oxygen atoms remain perfectly co-linear. The interested reader is referred to Fig. 8 along with Tables 6, 7, 8 for a detailed comparison of these two structures with that of the neutral compound (of O_h symmetry), as well as for useful information regarding adiabatic relaxation energies from the vertical ionized state (ΔE_{rel}), and changes in frontier orbital energies due to the lowering of the symmetry point group. We note that releases of orbital energy degeneracies from the triply degenerate (T_{2g}) HOMO of the neutral into singly (A_{1g})

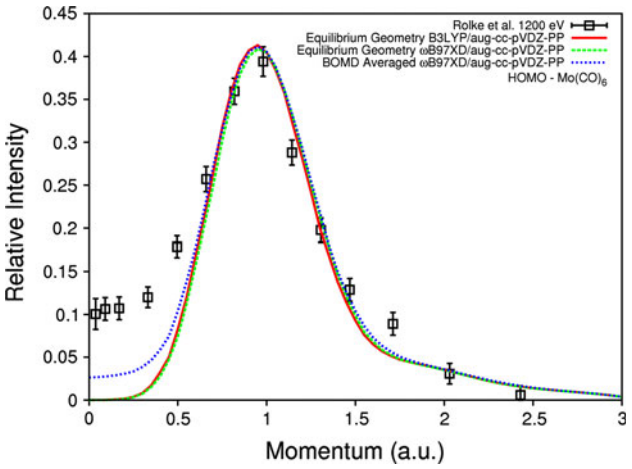

Fig. 7 Resolution folded ($E_0 = 1{,}200$ eV, $\Delta\theta = 0.60°$, $\Delta\phi = 1.20°$) and spherically averaged theoretical momentum distribution inferred for the HOMO of $Mo(CO)_6$ ($\varepsilon = 8.5$ eV), taking care of complications pertaining to nuclear dynamics in the initial state

and doubly degenerate (E_g) orbitals upon imposing the D_{3d} structures of the cation do not exceed 0.15 eV. Since these levels cannot be individually resolved in EMS experiments, the corresponding momentum profiles have been summed to unravel the possible outcome of nuclear dynamics in the final state.

Upon examining Fig. 9, it is clear that final state dynamics associated with the Jahn–Teller distortions and release of symmetry constraints induced upon removal of an electron from the triply degenerate $2t_{2g}$ orbital of $W(CO)_6$ is also quite likely to induce a turn-up in the experimentally inferred momentum profiles for the $2t_{2g}^{-1}$ ionization channel, especially when considering the frontier momentum distribution for the adiabatically relaxed structure characterized by $\tau = 57.6°$. This turn-up arises because of the admixture of a fully symmetric (A_{1g}) orbital contribution (Table 8). Here again, this turn-up is on its own too weak to enable us to quantitatively reproduce experiment. Assuming a fully adiabatic ionization process, nuclear dynamics in the final state cannot account for more than one-third of the experimentally observed (e, 2e) ionization intensities at $p \to 0$. At this stage, it is worth reminding that such a depiction certainly overestimates the changes in the momentum densities induced by geometrical relaxation in the final state, during a real, that is, on a finite time scale, (e, 2e) ionization process. We note also that, within an adiabatic depiction, a Jahn–Teller distortion of the molecular structure of $W(CO)_6$ into a slightly flattened geometry characterized by $\tau = 53.5°$ only results in a barely visible turn-up (Fig. 9) in the low momentum region. Exactly the same remarks can be made (Figs. 10, 11) regarding the influence of nuclear dynamics in the final ionized state upon the momentum profile characterizing the HOMO of $Cr(CO)_6$ and $Mo(CO)_6$.

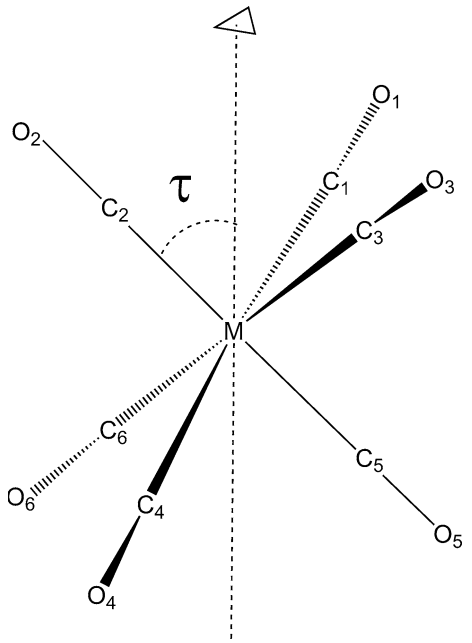

Fig. 8 Main geometrical parameters of the target group 6b metal hexacarbonyl compounds and of their radical cation

At last, it is worth noticing that on the experimental side [45], increasing the electron impact energy from 1.2 to 2.4 keV does have a small albeit discernable effect on the recorded momentum distributions for the HOMO of tungsten hexacarbonyl (Fig. 9). Note, in particular, that the agreement between theory and experiment slightly improves (beyond the reported statistical error [45]) at low momenta when resorting to an impinging electron beam with $E_0 = 2.4$ keV. In view of the *d*-like topology of the HOMO, which exhibits two perpendicular nodal planes intersecting at the location of the heavy metal atom, along with π-contributions from the CO groups (Fig. 12), it seems thus quite likely that, in spite of the negative conclusions by Liu et al. [45], distorted wave effects do play a role and converge more slowly upon increasing electron impact energies, than in the case of isolated atoms, due to the presence of many (13) scattering interference atomic centers in a target like $W(CO)_6$. The reader's attention is drawn on the fact that, whereas larger relative (e, 2e) intensities are obtained at low momenta when $E_0 = 1.2$ keV, significantly lower relative (e, 2e) intensities are on the contrary observed for the peak at $\sim$0.9 a.u., compared with the results obtained at an impact energy of 2.4 keV. All in all, the experimental frontier momentum profile of $W(CO)_6$ seems thus far from being fully converging when E_0 increases from 1.2 to 2.4 keV. Note also that DWIA calculations indicate that, instead of vanishing as it should by virtue of symmetry constraints, the low momentum "turn-up" in the (e, 2e) ionization cross-sections for the 3d level of an atomic target like Ti still remains very prominent even at $E_0 = 2.4$ keV [44, 46]. Electron impact energies of the order of 10 keV or more might therefore be necessary for ensuring the convergence

Table 6 Comparison of the molecular geometries and frontier electronic structure of $Cr(CO)_6$ in its neutral ground state and lowest ionized (radical cation) state

Structure	τ (°)	R[Cr–C] in Å	R[C–O] in Å	$\theta(C_1–Cr–C_3)$ in °	$\theta(C_3–Cr–C_4)$ in °	ΔE^a_{rel} (kcal/mol)	Frontier orbitals and their energies (eV)
O_h (neutral)	54.7	1.925	1.148	90.0	90.0	–	7.165 (T_{2g})
D_{3d} (1) (cation)	57.2	2.000	1.133	86.6	93.4	−8.333	6.583 (A_{1g})
							6.736 (E_g)
D_{3d} (2) (cation)	53.6	2.000	1.133	91.6	88.4	−7.096	6.663 (E_g)
							6.729 (A_{1g})

[a] Adiabatic relaxation energy from the vertical ionized state

Table 7 Comparison of the molecular geometries and frontier electronic structure of $Mo(CO)_6$ in its neutral ground state and lowest ionized (radical cation) state

Structure	τ (°)	R[Mo–C] in Å	R[C–O] in Å	$\theta(C_1–Mo–C_3)$ in °	$\theta(C_3–Mo–C_4)$ in °	ΔE^a_{rel} (kcal/mol)	Frontier orbitals and their energies (eV)
O_h (neutral)	54.7	2.076	1.147	90.0	90.0	–	7.046 (T_{2g})
D_{3d} (1) (cation)	57.7	2.127	1.134	85.8	94.2	−6.056	6.591 (A_{1g})
							6.784 (E_g)
D_{3d} (2) (cation)	53.5	2.127	1.134	91.8	88.2	−4.693	6.699 (E_g)
							6.771 (A_{1g})

[a] Adiabatic relaxation energy from the vertical ionized state

Table 8 Comparison of the molecular geometries and frontier electronic structure of $W(CO)_6$ in its neutral ground state and lowest ionized (radical cation) states

Structure	τ (°)	R[W–C] in Å	R[C–O] in Å	$\theta(C_1–W–C_3)$ in °	$\theta(C_3–W–C_4)$ in °	ΔE^{a}_{rel} (kcal/mol)	Frontier orbitals and their energies (eV)
O_h (neutral)	54.7	2.072	1.149	90.0	90.0	–	7.063 (T_{2g})
D_{3d} (1) (cation)	57.6	2.114	1.136	86.1	93.9	−5.531	6.651 (A_{1g})
							6.839 (E_g)
D_{3d} (2) (cation)	53.5	2.114	1.136	91.8	88.2	−4.161	6.753 (E_g)
							6.831 (A_{1g})

[a] Adiabatic relaxation energy from the vertical ionized state

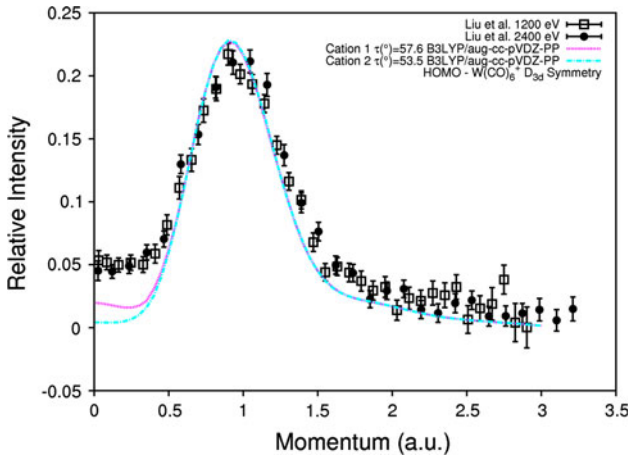

Fig. 9 Resolution folded ($E_0 = 2{,}400$ eV, $\Delta\theta = 0.53°$, $\Delta\phi = 0.84°$) and spherically averaged theoretical momentum distribution inferred for the HOMO of $W(CO)_6$ ($\varepsilon = 8.6$ eV), taking care of complications pertaining to nuclear dynamics in the initial states

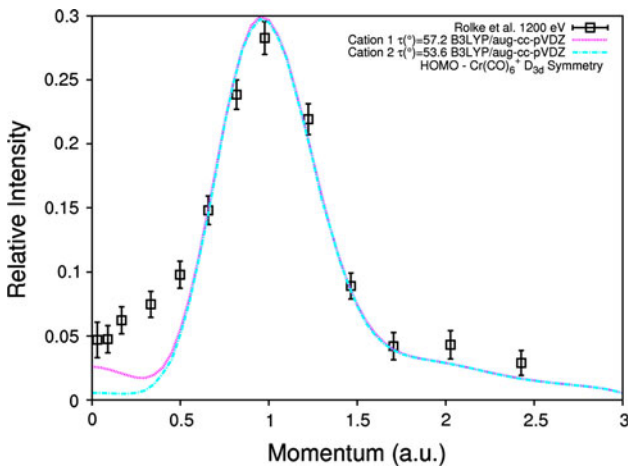

Fig. 10 Resolution folded ($E_0 = 1{,}200$ eV, $\Delta\theta = 0.60°$, $\Delta\phi = 1.20°$) and spherically averaged theoretical momentum distribution inferred for the HOMO of $Cr(CO)_6$ ($\varepsilon = 8.4$ eV), taking care of complications pertaining to nuclear dynamics in the initial states

of the momentum profiles of $W(CO)_6$, $Cr(CO)_6$, and $Mo(CO)_6$ to the high energy limit [102], at which the plane wave impulse approximation becomes valid.

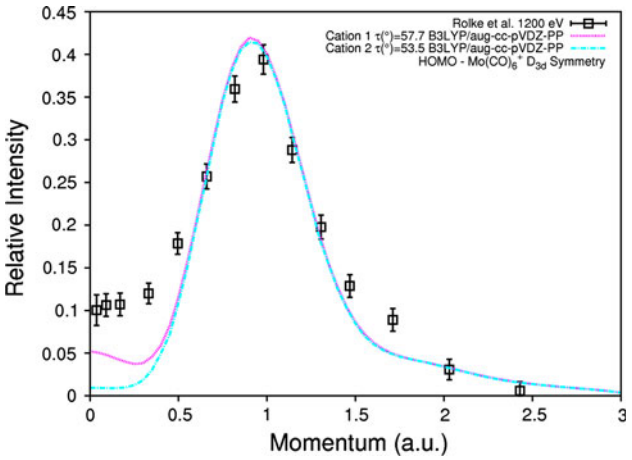

Fig. 11 Resolution folded ($E_0 = 1{,}200$ eV, $\Delta\theta = 0.60°$, $\Delta\phi = 1.20°$) and spherically averaged theoretical momentum distribution inferred for the HOMO of $Mo(CO)_6$ ($\varepsilon = 8.5$ eV), taking care of complications pertaining to nuclear dynamics in the initial states

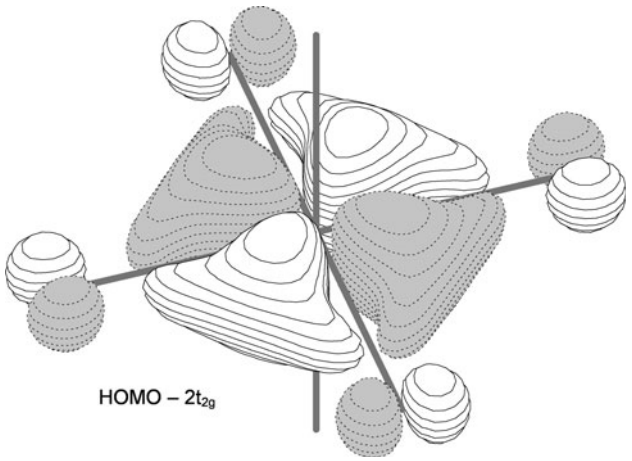

Fig. 12 Contour plot (contour value equal to 0.05) of the triply degenerate HOMO ($2t_{2g}$) of $W(CO)_6$ (this figure was made using MOLDEN [89])

5 Conclusions

The origin of the turn-up in the (e, 2e) ionization intensities which has been experimentally detected [43–45] in EMS

studies at low electron momenta for the HOMO of group 6 (W, Cr, Mo) hexacarbonyl compounds has been reinvestigated, on the basis of large-scale calculations using the target Kohn–Sham approximations along with the standard hybrid B3LYP and dispersion-corrected ωB97XD exchange–correlation functionals. Our study invalidates the view [45] that the unexpectedly large (e, 2e) frontier orbital densities that were experimentally inferred in the low momentum region can be solely explained by nuclear displacements associated with the first three triply degenerate vibrational eigenmodes of these compounds. Indeed, at room temperature, an analysis of populations over these three vibrational eigenmodes ($1T_{2u}$, $1T_{1u}$, $1T_{2g}$) according to (Maxwell-)Botzmann thermostatistics indicate that these motions can only account for a very marginal fraction (a few % at most) of (e, 2e) ionization cross-sections at $p \rightarrow 0$.

Two different scenarios invoking nuclear dynamics in the initial ground state and nuclear dynamics in the final ionized state have been tested, on the ground of two very opposite models, assuming a vertical and an adiabatic depiction of the (e, 2e) reaction process, respectively. Both dynamics may partly contribute to the turn-up of (e, 2e) ionization intensities of the HOMO in the low momentum region, but none of them is on its own sufficient to explain this very large turn-up. Indeed, simulations employing Born–Oppenheimer molecular dynamics demonstrate that, at or near standard temperatures ($T = 298$ K or $T = 310$ K), thermally induced molecular motions on the potential energy surface associated with the electronic ground state can account for, at most, one-third of the experimentally observed (e, 2e) ionization cross-sections at $p \rightarrow 0$. Also, nuclear dynamics in the final state, in the form of Jahn–Teller distortions, can also only at best contribute for about the same ratio to these experimental cross-sections at or near zero electron momentum. In view of small but clearly observable differences in between EMS measurements at electron impact energies of 1.2 and 2.4 keV (Fig. 9), the only possible explanation we are left with is that both types of dynamical complications as well as distorted wave and post-collision (rescattering) effects in the continuum *cumulate* and yield *altogether* the experimentally observed turn-ups. Further EMS measurements, at much larger electron impact energies, with femtosecond time resolution as well as upon ultra-cooled supersonic molecular beams, are very much needed therefore for disentangling all these physical effects in a proper way on the experimental side. On theoretical side, the present study also most clearly emphasizes the need of thorough methodological and computational developments for quantitatively interpreting molecular EMS experiments upon large polyatomic systems beyond the plane wave impulse approximation. At the moment, a promising but still unexplored solution for investigating distorted wave effects in these systems consists in a molecular extension [6] of the BBK (Brauner, Briggs, and Klar) model [103] for the ionization of atoms.

Acknowledgments All calculations that were presented in this work have been performed on Compaq (HP) ES45 and ES47 workstations at Hasselt University, Belgium, and at the Flemish Supercomputer Center (Vlaams Supercomputer Centrum). This work has been supported by the FWO-Vlaanderen, the Flemish branch of the Belgian National Science Foundation, and by the Bijzonder OnderzoeksFonds of Hasselt University. The authors especially acknowledge financial support from a Research Program of the Research Foundation—Flanders (FWO_Vlaanderen; project number G.0350.09N, entitled "*From orbital imaging to quantum similarity in momentum space*").

References

1. McCarthy IE, Weigold E (1991) Rep Prog Phys 54:789
2. Coplan MA, Moore JH, Doering JP (1994) Rev Mod Phys 66:985
3. Weigold E, McCarthy IE (1999) Electron Momentum Spectroscopy. Kluwer, New York
4. Neudatchin VG, Popov YV, Smirnov YF (1999) Physics-Uspehki 42:1017
5. Pang WN, Gao JF, Ruan CJ, Shang RC, Trofimov AB, Deleuze MS (2000) J Chem Phys 112:8043
6. Stia CR, Fojon OA, Weck PF, Hanssen J, Joulakian B, Rivarola RD (2002) Phys Rev A 66:052709
7. Champion C, Cappello CD, Houamer S, Mansouri A (2006) Phys Rev A 73:012717
8. Pickup BT (1977) Chem Phys 19:193
9. Öhrn Y (1981) Adv Quantum Chem 13:1
10. Deleuze M, Pickup BT, Delhalle J (1994) Mol Phys 83:655
11. Seabra GM, Kaplan IG, Zakrzewski VG, Ortiz JV (2004) J Chem Phys 121:4143
12. Duffy P, Chong DP, Casida ME, Salahub DR (1994) Phys Rev A 50:4704
13. Deleuze MS, Cederbaum LS (1997) Int J Quantum Chem 63:465
14. Golod A, Deleuze MS, Cederbaum LS (1999) J Chem Phys 110:6014
15. Ning CG, Ren XG, Deng JK, Su GL, Zhang SF, Knippenberg S, Deleuze MS (2006) Chem Phys Lett 421:52
16. Ning CG, Hajgató B, Huang YR, Zhang SF, Liu K, Luo ZH, Knippenberg S, Deng JK, Deleuze MS (2008) Chem Phys 343:19
17. Knippenberg S, François JP, Deleuze MS (2006) J Comp Chem 27:1703
18. Shojaei SHR, Hajgató B, Deleuze MS (2010) Chem Phys Lett 498:45
19. Deleuze MS, Pang WN, Salam A, Shang RC (2001) J Am Chem Soc 123:4049
20. Knippenberg S, Huang YR, Hajgató B, François JP, Deng JK, Deleuze MS (2007) J Chem Phys 127:174306
21. Morini F, Knippenberg S, Deleuze MS, Hajgató B (2010) J Phys Chem A 114:4400
22. Hajgató B, Deleuze MS, Morini F (2009) J Phys Chem A 113:7138
23. Takahashi M, Ogino R, Udagawa Y (1998) Chem Phys Lett 288:821
24. Ehara M, Ohtsuka Y, Nakatsuji H, Takahashi M, Udagawa Y (2005) J Chem Phys 122:234319

25. Deleuze MS, Knippenberg S (2006) J Chem Phys 125:104309
26. Huang CW, Shan X, Zhang Z, Wang EL, Li ZJ, Chen XJ (2010) J Chem Phys 133:124303
27. Brion CE, Zheng Y, Rolke J, Neville JJ, McCarthy IE, Wang J (1998) J Phys B 31:L223
28. Takahashi M, Saito T, Hiraka J, Udagawa Y (2003) J Phys B 36:2539
29. Nixon KL, Lawrance WD, Brunger MJ (2009) Chem Phys Lett 474:23
30. Takahashi M, Khajuria Y, Udagawa Y (2003) Phys Rev A 68:042710
31. Watanabe N, Takahashi M, Udagawa Y, Kouzakov KA, Popov YV (2007) Phys Rev A 75:052701
32. Takahashi M, Miyake Y, Watanabe N, Udagawa Y, Sakai Y, Mukoyama T (2007) Phys Rev Lett 98:013201
33. Ren XG, Ning CG, Deng JK, Zhang SF, Su GL, Huang F, Li GQ (2005) Phys Rev Lett 94:163201
34. Knippenberg S, Deleuze MS, Cleij TJ, François JP, Cederbaum LS, Eland JHD (2005) J Phys Chem A 109:4267
35. Knippenberg S, Hajgató B, François JP, Deleuze MS (2007) J Phys Chem A 111:10834
36. Knippenberg S, Hajgató B (2012) Spectrochim Acta A 102:2012
37. Li ZJ, Chen XJ, Shan X, Liu T, Xu KZ (2009) J Chem Phys 130:054302
38. Mingos DMP (1982) In: Wilkinson G (ed) Comprehensive organometallic chemistry, vol 3 of Comprehensive organometallic chemistry. Pergamon Press, New York
39. Huheey JE (1983) Inorganic chemistry: principles of structure and reactivity, 3rd edn. Harper International SI Edition, Cambridge
40. Cotton FA, Wilkinson G (1988) Advanced inorganic chemistry, 5th edn. Wiley-Interscience, New York
41. Schriver DF, Atkins PW (2006) Inorganic chemistry, 4th edn. Oxford University Press, Oxford
42. Higginson BR, Lloyd DR, Burroughs P, Gibson DM, Orchard AF (1973) J Chem Soc Faraday Trans 2:69
43. Chornay DJ, Coplan MA, Tossell JA, Moore JR, Baerends EJ, Rozendaal A (1985) Inorg Chem 24:877
44. Rolke J, Zheng Y, Brion CE, Chakravorty SJ, Davidson ER, McCarthy IE (1997) Chem Phys 215:191
45. Liu K, Ning CG, Luo ZH, Shi LL, Deng JK (2010) Chem Phys Lett 497:229
46. Brunger MJ, Braidwood SW, McCarthy IE, Weigold E (1994) J Phys B 27:L597
47. Takahashi M, Udagawa Y (2004) J Electron Spectrosc Rel Phenom 137:187
48. Landau LD, Lifshitz EM (1977) Quantum mechanics: non-relativistic theory. Pergamon, Oxford
49. Nicholson RJF, McCarthy IE, Weyrich W (1999) J Phys B 32:3873
50. Miyake Y, Takahashi M, Watanabe N, Khajuria Y, Udagawa Y, Sakai Y, Mukoyama T (2006) Phys Chem Chem Phys 8:3022
51. Champion C, Hanssen J, Hervieux PA (2002) Phys Rev A 65:022710
52. Builth-Williams JD, Bellm SM, Jones DB, Chaluvadi H, Madison DH, Ning CG, Lohmann B, Brunger MJ (2012) J Chem Phys 136:024304
53. McQuarrie DA (2000) Statistical mechanics. University Science Books, Sausalito
54. Carter AH (2001) Classical and statistical thermodynamics. Prentice Hall, Upper Saddle River
55. Helgaker T, Uggerud E, Jensen HJA (1990) Chem Phys Lett 173:145
56. Uggerud E, Helgaker T (1992) J Am Chem Soc 114:4265
57. Bolton K, Hase WL, Peslherbe GH (1998) In: Thompson DL (ed) Modern methods for multidimensional dynamics computation in chemistry. World Scientific, Singapore, p 143
58. Haile JMP (1997) Molecular dynamics simulation. Wiley, New York
59. Williams RW, Heilweil EJ (2010) Chem Phys 373:251
60. Joalland B, Rapacioli M, Simon A, Joblin C, Mardsen CJ, Spiegelman F (2010) J Phys Chem A 114:5846
61. Simon A, Rapacioli M, Lanza M, Joalland B, Spiegelman F (2011) Phys Chem Chem Phys 13:3359
62. Ramírez-Solís A, Jolibois F, Maron L (2011) Chem Phys Lett 510:21
63. Ning CG, Luo ZH, Huang YR, Hajgató B, Morini F, Liu K, Zhang SF, Deng JK, Deleuze MS (2008) J Phys B 41:175103
64. Levin VG, Neudatchin VG, Pavlitchenkov AV, Smirnov YF (1975) J Chem Phys 63:1541
65. Venkatesan TS, Mahapatra S, Cederbaum LS, Köppel H (2004) J Phys Chem A 108:2256
66. Köppel H, Domcke W, Cederbaum LS (1984) Adv Chem Phys 57:59
67. Deleuze MS, Hajgató B, Morini F, Knippenberg S (2010) J Phys Conf Ser 212:012020
68. Parr RG, Yang W (1989) Density functional theory of atoms and molecules. Oxford University Press, New York
69. Becke AD (1993) J Chem Phys 98:5648
70. Lee C, Yang W, Parr RG (1988) Phys Rev B 37:785
71. Chai JD, Head-Gordon M (2008) Phys Chem Chem Phys 10:6615
72. Dunning TH Jr (1989) J Chem Phys 90:1007
73. Kendall RA, Dunning TH Jr, Harrison R (1992) J Chem Phys 96:6796
74. Peterson K, Figgen D, Dolg M, Stoll H (2007) J Chem Phys 126:124101
75. Figgen D, Peterson KA, Dolg M, Stoll H (2009) J Chem Phys 130:164108
76. Peterson KA (2003) J Chem Phys 119:11099
77. Odoh OS, Schreckenbach G (2010) J Phys Chem A 114:1957
78. Frisch MJ, Trucks GW, Schlegel HB, Scuseria GE, Robb MA, Cheeseman JR, Scalmani G, Barone V, Mennucci B, Petersson GA, Nakatsuji H, Caricato M, Li X, Hratchian HP, Izmaylov AF, Bloino J, Zheng G, Sonnenberg JL, Hada M, Ehara M, Toyota K, Fukuda R, Hasegawa J, Ishida M, Nakajima T, Honda Y, Kitao O, Nakai H, Vreven T, Montgomery JA Jr., Peralta JE, Ogliaro F, Bearpark M, Heyd JJ, Brothers E, Kudin KN, Staroverov VN, Kobayashi R, Normand J, Raghavachari K, Rendell A, Burant JC, Iyengar SS, Tomasi J, Cossi M, Rega N, Millam JM, Klene M, Knox JE, Cross JB, Bakken CV, Jaramillo J, Gomperts R, Stratmann RE, Yazyev O, Austin AJ, Cammi R, Pomelli C, Ochterski JW, Martin RL, Morokuma K, Zakrzewski VG, Voth GA, Salvador P, Dannenberg JJ, Dapprich S, Daniels AD, Farkas Ö, Foresman JB, Ortiz JV, Cioslowski J, Fox DJ (2009) Gaussian 09, Revision B.1. Gaussian, Inc., Wallingford
79. Ren XG, Ning CG, Deng JK, Zhang SF, Su GL, Huang F, Li GQ (2005) Rev Sci Instrum 76:063103
80. Casida ME (1995) Phys Rev A 51:2005
81. Gritsenko OV, Braïda B, Baerends EJ (2003) J Chem Phys 119:1937
82. Janak JF (1978) Phys Rev B 18:7165
83. Vanfleteren D, Van Neck D, Ayers PW, Morrison RC, Bultinck P (2009) J Chem Phys 130:194104
84. Bawagan AO (1987) Ph.D. Thesis, University of British Columbia (UBC). See various contributions to the original HEMS program as recorded by Bawagan. The HEMS (now known as MOMAP) program has been extensively revised and extended at UBC by Cann NM and Cooper G
85. Duffy P, Casida ME, Brion CE, Chong DP (1992) Chem Phys 159(b):347
86. Bawagan AO, Brion CE (1990) Chem Phys 144:167
87. Bulirsch R, Stoer J (1991) Introduction to numerical analysis. Springer, New York

88. Press WH, Flannery BP, Teukolsky SA, Vetterling WT (1992) Richardson extrapolation and the Bulirsch-Stoer method. In: Numerical recipes in FORTRAN: the art of scientific computing. Cambridge University Press, Cambridge, 2nd edn., pp 718–725
89. Schaftenaar G, Noordik JH (2000) J Comput-Aided Mol Des 14:123
90. Vanlenthe E, Baerends E, Snijders J (1994) J Chem Phys 101:9783
91. Ehlers AW, Frenking G (1993) J Chem Soc Chem Commun 1709
92. Jonas V, Frenking G, Reetz MT (1992) J Comput Chem 13:919
93. Hay PJ, Wadt WR (1985) J Chem Phys 82:299
94. Hehre WJ, Ditchfield R, Pople PA (1972) J Chem Phys 56:2257
95. Shimanouchi T, Molecular vibrational frequencies. In: Lingstrom PJ, Mallard WG (eds) NIST Chemistry WebBook, NIST Standard Reference Database Number 69, National Institute of Standards and Technology, Gaithersburg MD, 20899, http://webbook.nist.gov
96. Shimanouchi T (1972) J Phys Chem Ref Data 6:993
97. Bérces A (1996) J Phys Chem A 100:16538
98. Mortimer RG (2003) Physical Chemistry, 3rd edn. Elsevier, London
99. Mc Quarrie DA, Simons JD (1997) Physical chemistry—a molecular approach. University Science Books, Sausalito
100. Atkins P, de Paula J (2010) Physical Chemistry, 9th edn. W. H. Freeman, New York
101. Herzberg G (1956) Molecular spectra and molecular structure; Part II. Infrared and Raman Spectra of Polyatomic Molecules, 07th Printing. D. Van Nostrand Company, Princeton
102. Takahashi M (2010) Oral remark at the international conference on many-particle spectroscopy of atoms, molecules, clusters, and surfaces; (MPS2012), held in Sendai. Japan, Sendai, 4–7 September 2010
103. Brauner M, Briggs JS, Klar J (1989) J Phys B 22:2265